

CHEMISTRY

AN **ASIAN** JOURNAL

www.chemasianj.org

Accepted Article

Title: ZrMn oxides for aqueous-phase ketonization of acetic acid: effect of crystal and porosity

Authors: Kejing Wu, Mingde Yang, Husheng Hu, Junmei Liang, and Yulong Wu

This manuscript has been accepted after peer review and appears as an Accepted Article online prior to editing, proofing, and formal publication of the final Version of Record (VoR). This work is currently citable by using the Digital Object Identifier (DOI) given below. The VoR will be published online in Early View as soon as possible and may be different to this Accepted Article as a result of editing. Readers should obtain the VoR from the journal website shown below when it is published to ensure accuracy of information. The authors are responsible for the content of this Accepted Article.

To be cited as: *Chem. Asian J.* 10.1002/asia.201800114

Link to VoR: <http://dx.doi.org/10.1002/asia.201800114>

A Journal of



A sister journal of *Angewandte Chemie* and *Chemistry – A European Journal*

WILEY-VCH

ZrMn oxides for aqueous-phase ketonization of acetic acid: effect of crystal and porosity

Kejing Wu,^{[a], [b]} Mingde Yang,^{*[a]} Husheng Hu,^[a] Junmei Liang,^[a] Yulong Wu,^{*[a], [c]}

Abstract: Aqueous-phase ketonization of bio-based acetic acid is important to improve conversion efficiency of biomass resources. In this study, ZrMn mixed oxides (ZrMnO_x) with high aqueous-phase ketonization activity are synthesized through carbonization/oxidation method (COM) and solvothermal method (STM). The results show that ZrMnO_x prepared via COM possesses tetragonal ZrO₂, and hausmannite Mn₂O₃ is observed only at high oxidation temperature of 750 °C. Low-temperature and long-time oxidation results in decreased crystallinity and crystallite size, which is related to highly dispersed Mnⁿ⁺ species. The catalysts with improved acid sites possess high ketonization activity. Surface areas and pore size of ZrMnO_x synthesized via STM are controlled by the solvents for thermal treatment. Compared with water as solvent, ethanol benefits the increase in surface areas and pore size, resulting in high ketonization activity.

Introduction

Biomass resources, especially algae,^[1] possess promising potential to resolve energy and environmental concerns, such as depletion of fossil fuel reserves and greenhouse gas emissions.^[2] During hydrothermal conversion of biomass, large amount of acetic acid, one of major bio-based chemicals, exists in the aqueous-phase product.^[3] Pyrolysis of biomass also produces an aqueous fraction rich in acetic acid.^[4] Therefore, utilization of bio-based acids, especially acetic acid, is very important to improve conversion efficiency of biomass resources.^[5] An aqueous process can be used to convert acetic acid to liquid alkanes through ketonization, followed by aldol condensation and hydrogenation. The obtained hydrophobic liquid alkanes can directly be separated from water, avoiding separation costs of intermediate products during aqueous-phase conversion.^[5a] Huber et al.^[6] exhibited that aldol condensation of acetone and furfural, and subsequent hydrogenation could be efficiently achieved through aqueous catalysis. Thus,

ketonization is the crucial step for conversion of bio-based acetic acid in aqueous phase. Previous work^[1c, 1d] showed that hydrothermal liquefaction (HTL) at 300 – 400 °C efficiently converted algae to bio-oil. Aqueous-phase ketonization is feasible through applying similar reactors with HTL, and drawbacks of high temperature for efficient ketonization reaction may be resolved.

Generally, ketonization of acetic acid (with typical reaction equation of $2\text{CH}_3\text{COOH} \xrightarrow{\text{Cat.}} \text{CH}_3\text{COCH}_3 + \text{CO}_2 + \text{H}_2\text{O}$) is carried out in gas phase.^[7] However, gas-phase ketonization of acetic acid in aqueous phase requires large amount of energy for vaporization, which leads to low efficiency of overall energy recovery. Recently, ketonization in condensed toluene phase is achieved at 150 – 300 °C with high ketone yield.^[8] Because of the difficult extraction of aqueous-phase acetic acid and environmental concerns on organic solvents, organic-phase ketonization is also of low efficiency. Therefore, aqueous-phase ketonization is very important for the conversion of bio-based acetic acid.^[4b, 5a, 7a]

Recently, literatures on aqueous-phase ketonization of acetic acid over TiO₂ and ZrO₂ catalysts are available.^[4b, 9] Pham et al.^[4b] introduced a highly selective Ru/TiO₂/C catalyst and acid conversion was limited to 54.2 % after 5 h reaction because of irreversible deactivation. Faria et al. suggests that rutile TiO₂ decorated with Ru nanoparticles possesses high activity and stability.^[9a] However, noble metal Ru significantly increases synthesis cost of catalysts. Thus, it is necessary to develop non-noble catalysts for efficient aqueous-phase ketonization, and ZrO₂ is a promising candidate. Our previous work shows that carbon materials could efficiently promote aqueous-phase ketonization of acetic acid over ZrO₂ catalysts.^[9c] High acetone yield of 88.27% was achieved over non-noble ZrMn mixed oxides, and Mn leaching and crystal phase transformation were the main reasons of deactivation.^[9b] Because different synthesis methods result in varied crystal phase, pore properties and acid sites,^[8b] synthesis effect on ZrMn oxides should be investigated to understand relationship between aqueous-phase ketonization and catalyst properties.

Typically, two different methods are used to synthesize ZrMn oxides, namely citric acid method^[7e, 10] and co-precipitation method.^[11] Herein, carbonization process is applied for citric acid method to produce graphite carbon in catalysts.^[9c] Subsequently, different oxidation processes are used to remove carbon and control crystalline size and Mn dispersion. It is reported that hydrothermal treatment was efficient to synthesize mesoporous zirconium phosphate catalysts.^[12] Thus, solvothermal treatment is applied to controllably synthesize porous ZrMn oxides with higher surface areas and pore volumes/size than single co-precipitation method.^[11]

In this article, ZrMn oxide catalysts are controllably synthesized with different crystal phase, pore properties and acid sites for

[a] Dr. K.J. Wu, Dr. M.D. Yang, Master H.S. Hu, Dr. J.M. Liang, Dr. Y.L. Wu

Institute of Nuclear and New Energy Technology
Tsinghua University
Beijing 100084, China

E-mail: wylong@tsinghua.edu.cn; yangmd@tsinghua.edu.cn

[b] Dr. K.J. Wu
Institute of New Energy Low-Carbon Technology
Sichuan University
Chengdu 610065, China

[c] Dr. Y.L. Wu
Beijing Key laboratory of fine ceramics
Beijing 100084, China

Supporting information for this article is given via a link at the end of the document.

aqueous-phase ketonization of acetic acid. X-ray diffraction (XRD), N₂ absorption-desorption, NH₃ temperature-programmed desorption (NH₃-TPD), temperature-programmed reduction (TPR) and scanning electron microscopy (SEM) with energy dispersive X-ray (EDX) are applied for better understanding of relationship between catalyst characterization and activity.

Results and Discussion

Catalyst Characterization

XRD patterns of ZrMn-COM catalysts show typical tetragonal ZrO₂ (t-ZrO₂) (ICDD PDF No. 50-1089) with different crystallinity, as shown in Figure 1a. When oxidized at 350 and 550 °C, poorly crystallized t-ZrO₂ is similar with ZrMn-COM catalyst without oxidation. Sharp peaks are observed for ZrMn-COM-750-4, and a new phase of hausmannite Mn₃O₄ (ICDD PDF No. 24-0734) occurs. When oxidized at 750 °C for 24h, t-ZrO₂ peaks tend to be flatter. According to XRD data, peak parameters for the strongest (011) peak and related crystal parameters are calculated in Table 1. Peak positions of different catalysts have no significant differences with each other, but are larger than that of Zr-COM-350-4 (Figure S1 and Table S1). As no crystallized Mn species are observed for ZrMn-COM-350-4, Mnⁿ⁺ should exist in t-ZrO₂ crystal or be highly dispersed, and more discussions will be done in TPR results. Compared with Zr-COM-350-4, no monoclinic ZrO₂ is observed in ZrMn-COM catalysts, indicating that Mn species promote stabilization of t-ZrO₂.^[10] It is interesting that crystallite sizes of ZrMn-COM catalysts increase with temperature when oxidized for the same time, but decrease with oxidation time at the same temperature, as shown in Table 1.

Compared with ZrMn-COM-350-4 with the same oxidation process, ZrMn-STM catalysts possess only t-ZrO₂ phase with higher crystal peaks (Figure 1b). This result indicates co-precipitation and solvothermal treatment enhances crystallization of ZrO₂ phase. Meanwhile, the peak height decreases when using ethanol to replace water as solvent. Lattice distance of (011) facet increases in the order of W, W+Eth, Eth, while crystallite size decreases follow this order, as shown in Table 1. Thus, ethanol solvents will decrease ZrO₂ crystallization during solvothermal treatment.

Table 1. Crystal parameters of ZrMn-COM and ZrMn-STM catalysts.

Catalysts	2theta ^[a] (°)	d ^[a] of (011) (Å)	Crystallite size ^[b] (nm)
ZrMn-COM-None	30.55	2.924	3.5
ZrMn-COM-350-4	30.47	2.932	3.7
ZrMn-COM-350-24	30.55	2.924	3.5
ZrMn-COM-550-4	30.56	2.923	4.0
ZrMn-COM-550-24	30.51	2.928	3.6
ZrMn-COM-750-4	30.55	2.924	22.8
ZrMn-COM-750-24	30.39	2.939	13.2
ZrMn-STM-W	30.69	2.911	8.9
ZrMn-STM-W+Eth	30.61	2.918	8.3
ZrMn-STM-Eth	30.48	2.930	7.0

[a] 2theta and *d* (lattice distance) is the peak position of t-ZrO₂ (011) facet. [b] Crystallite size is calculated according to data of t-ZrO₂ (011) facet.

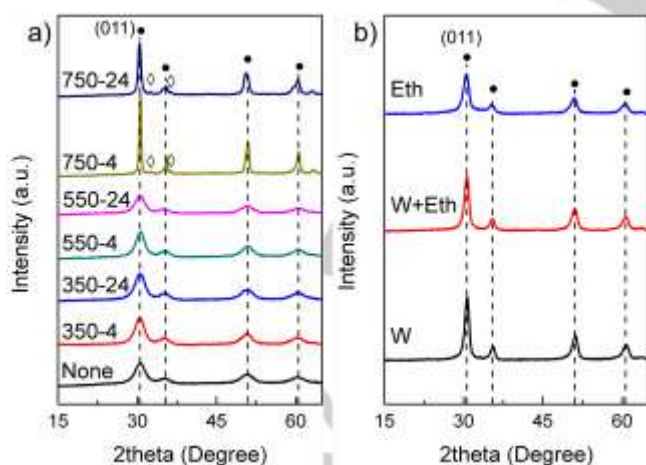


Figure 1. Figure 1. XRD patterns of ZrMn-COM catalysts oxidized at different temperature and time (a) and ZrMn-STM catalysts with different solvent (b). (●) refers to tetragonal ZrO₂, (○) refers to hausmannite Mn₃O₄. Only the strong and obvious peaks are noted and signal range is the same for (a) and (b).

As shown in Figure 2, TPR curve of ZrMn-COM-None is broad without typical peaks, which may result from the existence of carbon species (Figure S2), while TPR curves of oxidized ZrMn-COM catalysts possess identified peaks. Wide peaks from 175 to 400 °C are observed for ZrMn-COM-350(550), which are attributed to reduction of highly dispersed MnO_x.^[10, 11c, 13] Furthermore, two sub-peaks with different height near T₀ = 223 °C and T₁ = 303 °C can be observed through peak fitting. Considering the existence of Mn⁴⁺ and Mn³⁺,^[9b] sub-peak near T₀ is attributed to the reduction of Mn⁴⁺ species close to ZrO₂ phase, namely in ZrMn solid solution, and sub-peak near T₁ is related to aggregated 3-dimensional species of highly dispersed MnO_x.^[13] Differently, the TPR curve of ZrMn-COM-750-4 is broad without clear sub-peaks near T₀ and T₁. The combined peaks near 350 and 440 °C is attributed to reduction of MnO_x and Mn₃O₄, respectively.^[10, 13] The peak higher than 500 °C is related to ZrO₂ reduction.^[10] Complex reduction of MnO_x and ZrO₂ species results in the broad peak for ZrMn-COM-750-4. This result confirms that Mn species escape from highly crystallized ZrO₂ to form Mn₃O₄.

according to XRD results (Figure 1). However, TPR curve of ZrMn-COM-750-24 is similar with that oxidized at 350 and 550 °C, and a new peak is also observed near $T_2 = 406$ °C. Because Mn_3O_4 exists in ZrMn-COM-750-24 (Figure 1) and reduction of Mn_3O_4 is more difficult than MnO_2 and Mn_2O_3 ,^[13] sub-peak near T_2 should be attributed to the reduction of Mn_3O_4 to MnO .^[11c]

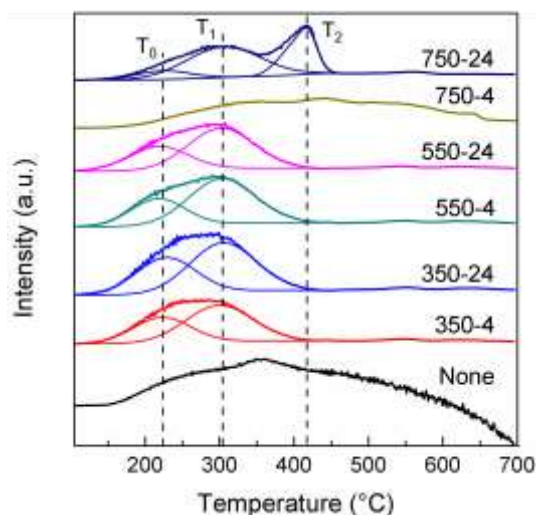


Figure 2. TPR curves of ZrMn-COM catalysts oxidized at different temperature and time, where None means no oxidation process.

Table 2. The normalized peak area of Mn species for ZrMn-COM catalysts according to TPR.

Catalysts	Sub-peak ^[a] area percentage (%)		
	T_0	T_1	T_2
ZrMn-COM-350-4	37.8	62.2	0
ZrMn-COM-350-24	40.2	59.8	0
ZrMn-COM-550-4	33.1	66.9	0
ZrMn-COM-550-24	36.1	63.9	0
ZrMn-COM-750-24	11.6	55.8	32.6

[a] Sub-peak of T_0 , T_1 and T_2 are 223, 303 and 406 °C, respectively.

The normalized sub-peak areas are listed in Table 2. Higher area percentage of T_0 indicates higher amount of highly dispersed MnO_x in solid solution. Obviously, higher oxidation temperature leads to lower MnO_x in solid solution, but longer oxidation time improves content of MnO_x species in solid solution. Because Mn^{n+} in ZrO_2 crystal has negative effect on crystallization,^[9b] high amount MnO_x in solid solution is accompanied by small crystallite size (Table 1). Meanwhile, escaped Mn^{n+} has potential to diffuse from individual Mn species

into ZrO_2 crystal, according to ZrMn-COM-750 oxidized for different time. Thus, highly dispersed MnO_x in ZrO_2 solid solution benefits the stability of t- ZrO_2 crystal and small crystal size.

N_2 absorption/desorption curves and average pore size distribution are shown in Figure 3. All isothermals of ZrMn-COM and ZrMn-STM catalysts can be classified as type IV with hysteresis loops at relative pressures ($P/P_0 > 0.8$), indicating the mesoporous structure caused by interparticle absorption.^[14] The pore size of different catalysts allocates mainly in two distributions of 2–3 nm and 10–20 nm. Pore size of ZrMn-STM increases gradually when using ethanol to replace water as thermal treatment solvent. ZrMn-COM-350-4 possesses much smaller pore size than ZrMn-STM catalysts, which is directly observed in Table 3. Surface areas and pore volumes of ZrMn-COM-350-4 (Table 3) are significantly larger than results in literature^[10], which confirms benefit of carbonization process. Without Mn species, Zr-COM-350-4 possesses much lower surface areas and pore volumes (Table S1), indicating significant enhancement of Mn species on surface properties.

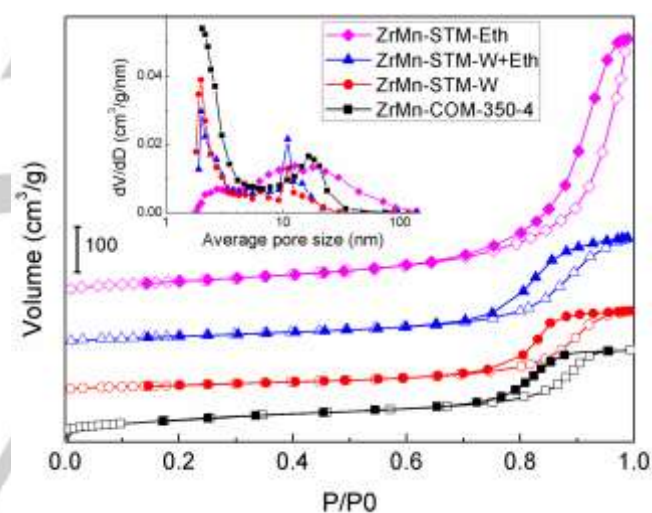


Figure 3. N_2 absorption and desorption curves of different catalysts. The offsets of ZrMn-STM-W, ZrMn-STM-W+Eth, and ZrMn-STM-Eth are 100, 200, and 300 cm^3/g , respectively. The open and filled symbols represent absorption and desorption data, respectively. The volume axis refers to 100 cm^3/g , and the inserted figure are related average pore size distribution.

As for different ZrMn-STM catalysts, morphology of irregular bulk particles is much similar, and surface Mn/Zr atom ratios are also similar with synthesized value of 0.4, as shown in Figure S3. The differences in surface areas of ZrMn-STM catalysts mainly result from thermal treatment solvents (Table 3). Thermal treatment with ethanol solvents can significantly improve surface areas and pore volumes over water solvent. During the thermal treatment, the organic solvents serve as templates for crystallization of ZrMn oxides, resulting in more mesoporous structure than water solvent. Higher surface areas and larger pore volumes/size would offer more surface active sites for ketonization reaction.

Table 3. Surface and pore properties of different catalysts.

Catalysts	$S_{\text{BET}}^{[a]}$ ($\text{m}^2 \text{g}^{-1}$)	$V_p^{[b]}$ ($\text{cm}^3 \text{g}^{-1}$)	$D_p^{[c]}$ (nm)
ZrMn-COM-350-4	158	0.309	7.83
ZrMn-STM-W	84	0.285	13.3
ZrMn-STM-W+Eth	106	0.376	13.7
ZrMn-STM-Eth	147	0.719	16.2

[a] BET surface areas. [b] Pore volumes. [c] Average pore size.

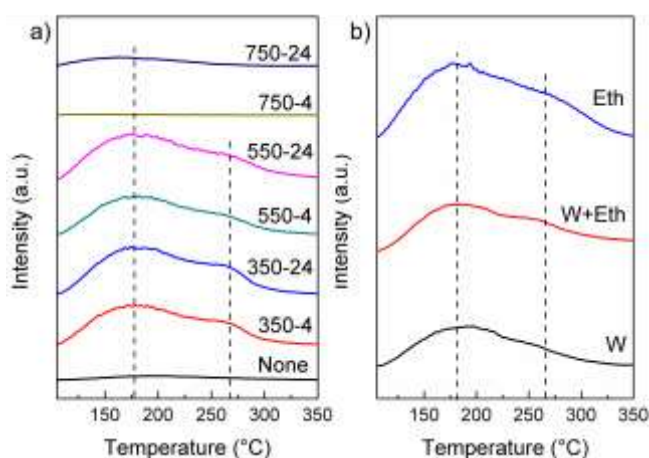


Figure 4. NH₃-TPD curves of ZrMn-COM catalysts (a) and ZrMn-STM (b). The intensity range is the same for (a) and (b).

The acid properties are analyzed via NH₃-TPD, as shown in Figure 4. No significant NH₃ desorption peak is observed for ZrMn-COM-None catalyst, and oxidation processes at 350 and 550 °C enhance acid properties (Figure 4a). Two peaks are significantly observed near 180 and 265 °C, representing different acid sites of the formation of NH₄⁺ on Brønsted acid sites and coordinated absorption on Lewis acid sites, respectively.^[10] However, peaks almost disappear for ZrMn-COM-750-4, and longer oxidation time results in weak NH₃ desorption peaks for ZrMn-COM-750-24. The total and Lewis acid sites are calculated as shown in Table 4. Oxidation at low temperature and long time benefits increase in acid sites. High total acid and Lewis acid sites are significantly accompanied by small crystallite size and highly dispersed MnO_x in ZrO₂ phase (Table 1 and 2). Meanwhile, ZrMn-COM-750-24 with high aggregated 3-dimensional MnO₂ content (T₁ in Table 2) possesses relatively less acid sites. Thus, aggregated 3-dimensional MnO₂ is not related to main acid sites. Therefore, poorly crystallized t-ZrO₂ incorporated with highly dispersed MnO_x, namely Zr-O-Mn, is the main acid site. Similarly, two

desorption peaks exist for ZrMn-STM catalysts (Figure 4b). The ethanol is a better solvent than water to increase total acid and Lewis acid sites (Table 4). High surface areas mainly devote to more surface Zr and Mn atoms and benefit increase in acid sites. However, S_{BET} of ZrMn-COM-350-4 catalyst is slightly higher than ZrMn-STM-Eth, but acid sites of the former is only half of the latter. The result is mainly attributed to the larger pore volumes and pore size of ZrMn-STM-Eth.

Table 4. Total and Lewis acid sites of ZrMn-COM and ZrMn-STM catalysts.

Catalysts	Total acid sites (mmol g^{-1})	Lewis acid sites ^[a] (mmol g^{-1})
ZrMn-COM-None	0.035	0.017
ZrMn-COM-350-4	0.373	0.141
ZrMn-COM-350-24	0.450	0.165
ZrMn-COM-550-4	0.360	0.114
ZrMn-COM-550-24	0.458	0.160
ZrMn-COM-750-4	0.009	0
ZrMn-COM-750-24	0.066	0.007
ZrMn-STM-W	0.342	0.089
ZrMn-STM-W+Eth	0.360	0.117
ZrMn-STM-Eth	0.732	0.228

[a] Lewis acid sites are calculated from the desorption areas at temperature range higher than middle position of 218 °C.

Ketonization Activity

The acetone yields of ZrMn-COM catalysts are shown in Figure 5. Maximum yield of 72.95% is observed for ZrMn-COM-350-24, which is significantly higher than that for noble Ru/TiO₂/C catalysts in aqueous phase.^[4b] Oxidation process at 350 and 550 °C significantly improve the acetone yield. When oxidation time increases from 4 to 24 h, crystallite size decreases and acid sites increase significantly for ZrMn-COM oxidized at both 350 and 550 °C, resulting in similar enhancement in acetone yield. However, activity becomes much low when oxidized at 750 °C for 4h. An obvious improvement of oxidation time on activity is observed, especially that acetone yield for ZrMn-COM-750-24 is three times of that for ZrMn-COM-750-4. Similarly prepared Mn-COM-350-4 and Zr-COM-350-4 both possess lower activity than ZrMn-COM-350-4 (Table S1), and acetone yield of Mn-COM-350-4 is only 4.7%. Our previous work showed that Mn leaching in aqueous acid solution was the deactivation process.^[9b] High Mn content in solid solution of ZrMn-COM-350-24 and ZrMn-COM-550-24 results in low Mn leaching at active sites (Table S2). Thus, high aqueous-phase ketonization of ZrMn-COM

catalysts is mainly resulted from interaction between Zr and Mn species, as shown in characterization results.

Highly dispersed Mn^{4+} in ZrO_2 crystal (T_0 reduction peak in Figure 2) contributes to more Zr-O-Mn sites than other Mn species. Meanwhile, two nearby acid molecules absorbed on Zr-O-Mn sites can easily form β -ketoacid, which is key intermediate for surface ketonization reaction^[9b]. However, acid molecules efficiently absorbed on highly dispersed aggregated 3-dimensional MnO_2 (T_1 reduction peak in Figure 2) are difficult to react without nearby Zr sites, as confirmed by low ketonization activity of Mn-COM-350-4. Besides, more Zr-O-Mn sites are accompanied with smaller crystal size and higher acid sites. Small ZrO_2 crystal possesses higher surface atoms, resulting in more active sites exposed on catalyst surface. Absorption of O atoms in acid molecules onto Lewis acid sites is crucial important for ketonization,^[4b] and high Lewis acid sites significantly improve aqueous-phase ketonization.^[7a] Therefore, Zr-O-Mn sites are recommended as main active centers, and suitable oxidation process can controllably increase content of Mn^{4+} highly dispersed in ZrO_2 crystal to improve the activity.

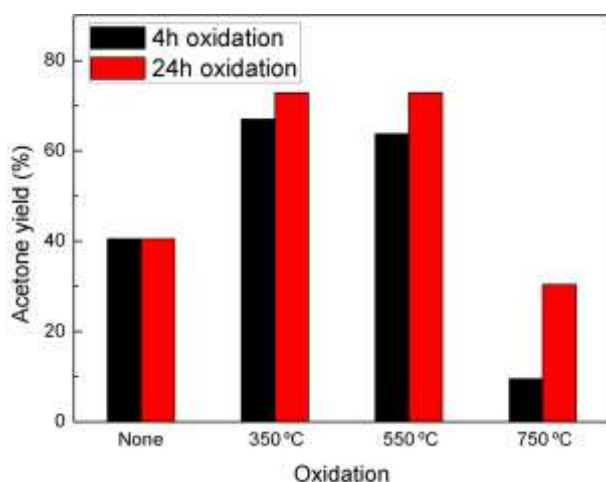


Figure 5. Acetone yield of ZrMn-COM oxidized at different temperature for 4 and 24 h. None refers to no oxidation.

Table 5. Acetone yields of ZrMn-STM catalysts thermally treated in different solvents.

Solvents	Acetone yield (%)	Acetone produced per total acid sites ^[a]
W	51.5	100
W+Eth	61.9	114
Eth	63.5	57.9

[a] Mole of acetone produced (mmol) is divided by the Lewis acid sites (mmol) of the added catalyst (1.5 g).

Despite the larger crystallite size than ZrMn-COM catalysts, activity of ZrMn-STM catalysts is still high (Table 5). Acetone yield increases when using ethanol to replace water as thermal treatment solvent, due to increase in surface areas and acid sites. According to literature,^[7a] Lewis acid sites, rather than Brønsted acid sites, are crucial important for ketonization. Acetone production per total acid sites is listed in Table 5. The results show that acetone production per total acid sites of ZrMn-STM-W+Eth is higher than that of ZrMn-STM-W, which is resulted from higher Lewis acid sites (Table 4). Considering the similar total acid sites, the higher performance of ZrMn-STM-W+Eth can be explained that Lewis acid sites can absorb O atoms of acid molecule to promote acid ketonization on catalyst surface. The significantly low acetone production per total acid sites of ZrMn-STM-Eth might result from limitation of reactant concentration and accessibility to acid sites in aqueous phase. As for acetone yield, the results confirm that high surface areas and large pore volumes/size, accompanied with high acid sites, benefit the catalyst performance.

Acid conversion of ZrMn-STM-Eth at 340 °C for different reaction time is shown in Figure 6. The rate equation, $dX/dt = k \cdot C_0^{n-1} \cdot (1-X)^n$, is applied to fit the experiment data, where X is acid conversion, t is reaction time, C_0 is the initial acid concentration, n is reaction order, and k is rate constant. The result indicates that acid conversion satisfies first-order reaction ($n = 1$) with $k = 0.117 \text{ h}^{-1}$, rather than stoichiometric second-order reaction, which is in accordance with previous study.^[9b] Mn cations near Zr^{4+} at Zr-O-Mn sites can easily absorb acetic acid, and thus, bimolecular surface reaction of absorbed carboxylates is promoted.^[15] The fast formation of carboxylates between acetic acid and Mn species results in limited bimolecular reaction due to one molecule of acid absorbed on Zr cations. Thus, it is reasonable to observe a first-order ketonization of acetic acid in aqueous phase.

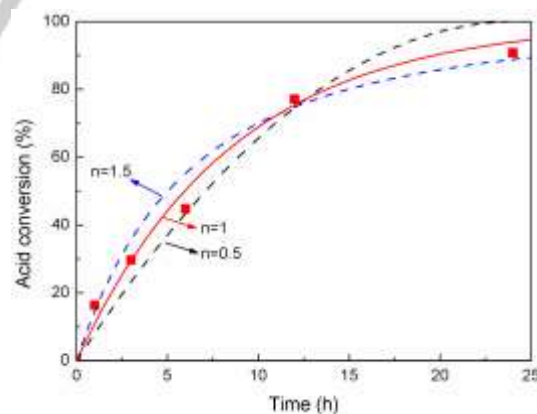


Figure 6. Acetone yield (dot) of ZrMn-STM-Eth at 340 °C for different reaction time. Three lines represent calculation value according to rate equation $dX/dt = k \cdot C_0^{n-1} \cdot (1-X)^n$ with different reaction order n (0.5, 1 and 1.5) and optimized reaction constant k (0.117 h^{-1}).

Conclusions

In this study, COM and STM are used to synthesize ZrMn mixed oxides catalyst for aqueous-phase ketonization. Crystal phase of ZrMn-COM catalysts can be controlled by oxidation process at different temperatures and times. Solvothermal treatment significantly affects surface areas and pore properties of ZrMn-STM catalysts. The results indicate that highly dispersed Mn species in t-ZrO₂ crystal phase promote the ketonization activity of ZrMn-COM catalysts. Small crystallite size benefits exposure of active Zr-O-Mn sites on catalyst surface, resulting in improved acid sites. Thermal treatment with ethanol solvent results in high surface areas and pore volumes/size, which benefit increase in acid site and ketonization activity. Controllable crystal and porous properties benefit the catalytic activity of ZrMn oxides synthesized via COM and STM for aqueous-phase ketonization of acetic acid.

Experimental Section

Catalyst preparation

As for carbonization/oxidation method (COM), 40 mmol Zr(NO₃)₄·5H₂O and 16 mmol Mn(NO₃)₂ were dissolved in 200 mL deionized water, and then, citric acid was added into the solution, mole of which equalled to four times of Zr⁴⁺ plus twice of Mn²⁺. The solution was vaporized at 90 °C under vigorous stirring to remove water, and yellow and viscous sol-gel was obtained. The sol-gel was dried at 105 °C for 24h to form a porous and foam-like solid, similarly with citric acid method. Subsequently, carbonization process was applied at 600 °C for 4h under 100 mL/min N₂. The dark solid was ground and sieved to 200 mesh. Finally, oxidation process was carried out under 100 mL/min air for 4 or 24h at different temperature (350, 550 and 750 °C). Here, different catalysts are marked as ZrMn-COM-Temperature-Time, for example, ZrMn-COM-350-4 means oxidized at 350 °C for 4h under 100 mL/min air, and ZrMn-COM-None refers to catalyst without oxidation treatment.

As for solvothermal method (STM), 24 mmol Zr(NO₃)₄·5H₂O and 9.6 mmol Mn(NO₃)₂ were dissolved to obtain an aqueous solution of 0.2 mol/L Zr⁴⁺, and the solution was transferred into a 500 mL beaker under vigorous stirring. Then, ammonia solution (25%) was dropped in the solution for completely precipitation, keeping a pH value of 10. After completely precipitation, the brown solid was aged for 24h, then filtered and washed with water until neutral pH. Subsequently, the filtered precipitation was dispersed in 100 mL solvent under ultrasonic, sealed in a 180 mL Teflon lining and thermal treated at 180 °C for 24h. Here, three kinds of solvents, water (W), water and ethanol mixture with volume ratio = 1:1 (W+Eth), and ethanol (Eth), were applied for thermal treatment. The obtained solid was filtered, dried, and calcined at 600 °C for 4h in 100 mL/min N₂ to totally remove solvent. Finally, ZrMn-STM catalysts were oxidized at 350 °C under 100 mL/min air for 4h. The catalysts are marked as ZrMn-STM-Solvent, according to the solvents used for thermal treatment.

Catalyst Characterization

XRD patterns were measured on a D8 ADVANCE diffractometer using CuKα radiation (λ=0.1541 nm, 36 kV, 2 mA) with a scanning step = 2 ° min⁻¹. The diffraction patterns were recorded by scanning at an angle ranging from 5 ° to 80 °. Peak fitting was applied to obtain the peak position and peak width of t-ZrO₂ (011) facet. Lattice distance and crystallite size were calculated through Bragg and Debye-Scherrer equations, respectively.

Morphological structure was identified using FEI Quanta 200F SEM with EDX spectra operating at 200 kV.

Surface area and pore volume were measured via N₂ absorption isotherms carried out on Tristar II 3020 (MICROMERITICS, United States) at 77K. Samples were pre-treated in vacuum at 300 °C. The specific surface areas were determined from Brunauer-Emmett-Teller (BET) equation, and pore volumes and average pore size were calculated using the Barrett-Joyner-Halenda (BJH) formula.

NH₃-TPD tests were carried out with a TP-5076 multifunctional automatic absorption instrument (Xianquan Industry and Trade Development Co., Tianjin, China). 100 mg sample was pre-treated at 350 °C for 1 h in He stream (30 mL/min) before ammonia absorption. After saturated absorption in the stream of pure NH₃ for 30 min, the sample was purged by He at 100 °C for 2 h to remove physisorbed ammonia. Then the TPD measurement was carried out from 100 to 350 °C with heating rate of 5 °C/min in He flow of 30 ml/min. The thermal conductivity detector was used for continuously monitoring the desorbed ammonia. The acid sites were measured via external standard of pure NH₃.

TPR experiments were similar with NH₃-TPD. Typically, 100 mg sample was pretreated at 350 °C for 1 h in He stream (30 mL/min), and after being cooled down to room temperature, a mixed H₂/N₂ gas (5% H₂) was used for TPR with a heating rate of 3 °C/min to 900 °C. A thermal conductivity detector was applied for H₂ signal detection.

Catalytic Activity Measurement

Measurements of aqueous-phase ketonization activity were similar with previous work [9b]. Briefly, 100 mL aqueous solution of 2 mol/L acetic acid and 1.5g catalyst were added in 500 mL steel batch reactor (Parr). The reactor was purged with 1 MPa N₂ for three times to remove existing air and finally pressured at 5 MPa N₂. The reactor was heated to 340 °C at a heating rate of 5 °C/min and kept for 12h under 300 rpm stirring. The pressure at 340 °C was about 19 MPa, which was higher than vapor-liquid pressure of water (14.5MPa) to maintain liquid phase reaction. The liquid product was collected after cooling down to room temperature, and acetone product and the remained acetic acid was quantified via GC analysis. Acetone was the mainly product in the aqueous phase, and acetone yields were calculated to measure catalyst activity.

Acknowledgements

This study was supported financially by National Natural Science Foundation of China (No. 21776159, No. 21576155 and No. 21376140), Research Project of Guangdong Provincial Department of Science and Technology Department (No. 2015B020215004) and Program for Changjiang Scholars and Innovative Research Team in University (No.IRT13026).

Keywords: Acetic acid • Aqueous-phase ketonization • ZrMn oxides • Oxidation • Solvothermal treatment

[1] a) M. Saber, B. Nakhshinie, K. Yoshikawa, *Renew. Sust. Energy Rev.* **2016**, *58*, 918-930; b) M. Ghadiryanfar, K. A. Rosentrater, A. Keyhani, M. Omid, *Renew. Sust. Energy Rev.* **2016**, *54*, 473-481; c) Y. Chen, Y. L. Wu, D. R. Hua, C. Li, M. P. Harold, J. L. Wang, M. D. Yang, *RSC Adv.* **2015**, *5*, 18673-18701; d) S. P. Zou, Y. L. Wu, M. D. Yang, C. Li, J. M. Tong, *Energy Environ. Sci.* **2010**, *3*, 1073-1078.

[2] a) D. M. Alonso, S. G. Wettstein, J. A. Dumesic, *Chem. Soc. Rev.* **2012**, *41*, 8075-8098; b) J. C. Serrano-Ruiz, R. Luque, A. Sepulveda-Escribano, *Chem. Soc. Rev.* **2011**, *40*, 5266-5281; c) A. A. Upadhye, W. Qi, G. W. Huber, *AIChE J.* **2011**, *57*, 2292-2301.

[3] a) G. Yu, Y. H. Zhang, L. Schideman, T. Funk, Z. C. Wang, *Energy Environ. Sci.* **2011**, *4*, 4587-4595; b) C. Gai, Y. H. Zhang, W. T. Chen, Y. Zhou, L. Schideman, P. Zhang, G. Tommaso, C. T. Kuo, Y. P. Dong, *Bioresour. Technol.* **2015**, *184*, 328-335; c) D. Zhou, L. A. Zhang, S. C. Zhang, H. B. Fu,

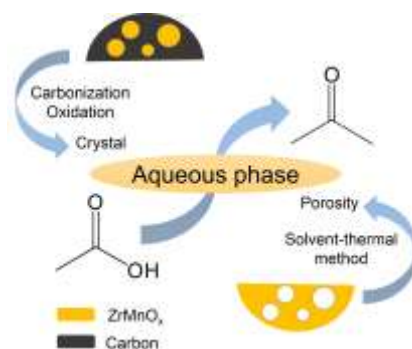
- J. M. Chen, *Energy Fuels* **2010**, *24*, 4054-4061; d) R. B. Madsen, M. M. Jensen, A. J. Morup, K. Houlberg, P. S. Christensen, M. Klemmer, J. Becker, B. B. Iversen, M. Glasius, *Anal. Bioanal. Chem.* **2016**, *408*, 2171-2183; e) B. Maddi, E. Panisko, K. Albrecht, D. Howe, *J. Vis. Exp.: JoVE* **2016**; f) E. Panisko, T. Wietsma, T. Lemmon, K. Albrecht, D. Howe, *Biomass Bioenergy* **2015**, *74*, 162-171.
- [4] a) R. Xing, V. L. Dagle, M. Flake, L. Kovarik, K. O. Albrecht, C. Deshmane, R. A. Dagle, *Catal. Today* **2016**, *269*, 166-174; b) T. N. Pham, D. C. Shi, T. Sooknoi, D. E. Resasco, *J. Catal.* **2012**, *295*, 169-178.
- [5] K. J. Wu, Y. L. Wu, Y. Chen, H. Chen, J. L. Wang, M. D. Yang, *ChemSusChem* **2016**, *9*, 1355-1385; b) C. A. Gärtner, J. C. Serrano-Ruiz, D. J. Braden, J. A. Dumesic, *ChemSusChem* **2009**, *2*, 1121-1124.
- [6] G. W. Huber, J. N. Chheda, C. J. Barrett, J. A. Dumesic, *Science* **2005**, *308*, 1446-1450.
- [7] a) T. N. Pham, T. Sooknoi, S. P. Crossley, D. E. Resasco, *ACS Catal.* **2013**, *3*, 2456-2473; b) M. Glinski, J. Kijenski, A. Jakubowski, *Appl. Catal. A* **1995**, *128*, 209-217; c) R. Pestman, R. M. Koster, A. vanDuijne, J. A. Z. Pieterse, V. Ponec, *J. Catal.* **1997**, *168*, 265-272; d) K. Parida, H. K. Mishra, J. Mol. Catal. A **1999**, *139*, 73-80; e) O. Nagashima, S. Sato, R. Takahashi, T. Sodesawa, *J. Mol. Catal. A* **2005**, *227*, 231-239; f) S. Eibner, A. Margeriat, F. Broust, D. Laurenti, C. Geantet, A. Julbe, J. Blin, *Appl. Catal. B* **2017**, *219*, 517-525.
- [8] a) R. W. Snell, S. H. Hakim, J. A. Dumesic, B. H. Shanks, *Appl. Catal. A* **2013**, *464*, 288-295; b) R. W. Snell, B. H. Shanks, *Appl. Catal. A* **2013**, *451*, 86-93; c) R. W. Snell, B. H. Shanks, *ACS Catal.* **2013**, *3*, 783-789; d) R. W. Snell, B. H. Shanks, *ACS Catal.* **2014**, *4*, 512-518.
- [9] a) N. Aranda-Pérez, M. P. Ruiz, J. Echave, J. Faria, *Appl. Catal. A* **2017**, *531*, 106-118; b) K. Wu, M. Yang, Y. Chen, W. Pu, H. Hu, Y. Wu, *AIChE J.* **2017**, *63*, 2958-2967; c) K. Wu, M. Yang, W. Pu, Y. Wu, Y. Shi, H.-s. Hu, *ACS Sustainable Chem. Eng.* **2017**, *5*, 3509-3516.
- [10] J. L. Zuo, Z. H. Chen, F. R. Wang, Y. H. Yu, L. F. Wang, X. H. Li, *Ind. Eng. Chem. Res.* **2014**, *53*, 2647-2655.
- [11] a) E. F. Lopez, V. S. Escribano, C. Resini, J. M. Gallardo-Amores, G. Busca, *Appl. Catal. B* **2001**, *29*, 251-261; b) J. K. Xie, Z. Qu, N. Q. Yan, S. J. Yang, W. M. Chen, L. G. Hu, W. J. Huang, P. Liu, *J. Hazard. Mater.* **2013**, *261*, 206-213; c) J. I. Gutierrez-Ortiz, B. de Rivas, R. Lopez-Fonseca, S. Martin, J. R. Gonzalez-Velasco, *Chemosphere* **2007**, *68*, 1004-1012.
- [12] L. Y. Cheng, X. K. Guo, C. H. Song, G. Y. Yu, Y. M. Cui, N. H. Xue, L. M. Peng, X. F. Guo, W. P. Ding, *RSC Adv.* **2013**, *3*, 23228-23235.
- [13] F. Arena, T. Torre, C. Raimondo, A. Parmaliana, *Phys. Chem. Chem. Phys.* **2001**, *3*, 1911-1917.
- [14] W. J. Roth, P. Nachtigall, R. E. Morris, P. S. Wheatley, V. R. Seymour, S. E. Ashbrook, P. Chlubná, L. Grajciar, M. Položij, A. Zukal, O. Shvets, J. Čejka, *Nature Chem.* **2013**, *5*, 628.
- [15] T. N. Pham, D. C. Shi, D. E. Resasco, *Top. Catal.* **2014**, *57*, 706-714.

Entry for the Table of Contents (Please choose one layout)

Layout 1:

FULL PAPER

ZrMnO_x is synthesized through carbonization/oxidation method with controlled crystal, and through solvothermal method with modified porosity. Crystal and porosity properties have significant influence on ketonization of acetic acid in aqueous phase.



Author(s), Corresponding Author(s)*

Page No. – Page No.

Title